

Capacitance Dispersion in n-LT-i-p GaAs Structures with the Low-Temperature Layers Grown at Different Temperatures

This content has been downloaded from IOPscience. Please scroll down to see the full text.

1999 Jpn. J. Appl. Phys. 38 L1425

(<http://iopscience.iop.org/1347-4065/38/12A/L1425>)

View [the table of contents for this issue](#), or go to the [journal homepage](#) for more

Download details:

IP Address: 140.113.38.11

This content was downloaded on 28/04/2014 at 08:43

Please note that [terms and conditions apply](#).

Capacitance Dispersion in n-LT-i-p GaAs Structures with the Low-Temperature Layers Grown at Different Temperatures

Jenn-Fang CHEN, Nie-Chuan CHEN, Pai-Yong WANG, Jiin-Shung WANG and Chi-Ming WENG

Department of Electrophysics, National Chiao Tung University, Hsinchu, Taiwan, R.O.C.

(Received September 16, 1999; accepted for publication October 13, 1999)

The electrical properties of annealed low-temperature GaAs are studied by investigating the frequency-dependent capacitance of n-LT-i-p structures with the low-temperature (LT) layers grown at different temperatures. Relative to the sample grown at 610°C, the samples grown at 200, 300 and 400°C show significant capacitance dispersions over frequency which is explained by the emission of carriers from traps. Based on a proposed band diagram where a dominating trap at 0.66–0.74 eV exists in the LT layers, the high-frequency dispersion is shown to be affected by resistance-capacitance (RC) time constant effects. From the mid-frequency capacitance versus voltage characteristics, the concentrations of the occupied traps are estimated to be $\approx 10^{17} \text{ cm}^{-3}$ for samples grown at 200, 300 and 400°C, which are found to be consistent with those obtained from analyzing the current-voltage characteristics of n⁺-LT-n⁺ structures.

KEYWORDS: low-temperature GaAs, deep levels, capacitance-frequency spectra

Recently, there has been considerable interest in understanding the underlying mechanisms^{1,2)} for the large resistivity and short carrier lifetime in low-temperature (LT) grown GaAs. A large concentration of defects such as As_{Ga} antisites^{3,4)} or various complexes⁵⁾ or arsenic precipitates²⁾ acting as buried Schottky barriers have been proposed. Despite these studies, the relative roles of different defects in rendering the LT GaAs high-resistivity and short lifetime still remains under contention. In our previous studies⁶⁾ on LT GaAs, dc resistivity measurements revealed the existence of a dominating trap at 0.66 eV below the conduction band, which is related to the semi-insulating property. In this work, we continue this study by carrying out the ac measurement on the electrical properties of LT GaAs grown at different temperatures.

The samples studied here are p-i-n GaAs diodes with part of the intrinsic layer grown at different temperatures. All samples were grown by a Varian Gen-II molecular beam epitaxy (MBE) system on n⁺-(001) GaAs substrates. The structure of the samples consists of 0.2 μm n($5 \times 10^{17} \text{ cm}^{-3}$)/0.2 μm undoped-layer grown at 200, 300, 400, and 600°C, respectively/0.6 μm intrinsic layer/0.4 μm p($1 \times 10^{17} \text{ cm}^{-3}$)/0.5 μm p⁺($> 10^{18} \text{ cm}^{-3}$). Besides the 0.2 μm undoped-layer, all the remaining layers were grown at 610°C. Details of the growth have been reported previously.⁶⁾ Figure 1 shows the current-voltage (*I*-*V*) characteristics at 376 K for the samples. All four samples show typical rectified *I*-*V* curves. The diameter of both diodes is 500 μm. It can be seen that the samples grown at 200, 300 and 400°C have similar reverse-bias currents which are higher compared to that of the sample grown at 600°C, indicating that the leakage current is increased by the existence of defects introduced by the LT growth.

Figure 2 shows the capacitance-frequency (C-F) spectra at a bias of -2 V for all the samples. Relative to the sample grown at 610°C, the samples grown at 200, 300 and 400°C show similar C-F spectra with two step-like capacitance dispersions over frequency. The low-frequency dispersion, where capacitance drops from $\approx 120 \text{ pF}$ to $\approx 40 \text{ pF}$, was previously identified to be the holes emitted from traps near the midgap.⁷⁾ Here, we are mainly interested in the high-frequency dispersion where capacitance drops from $\approx 40 \text{ pF}$ to $\approx 30 \text{ pF}$. According to the theory of admittance spectroscopy, the inverse of the frequency at which the capacitance drops corresponds to the emission time of carriers from traps,

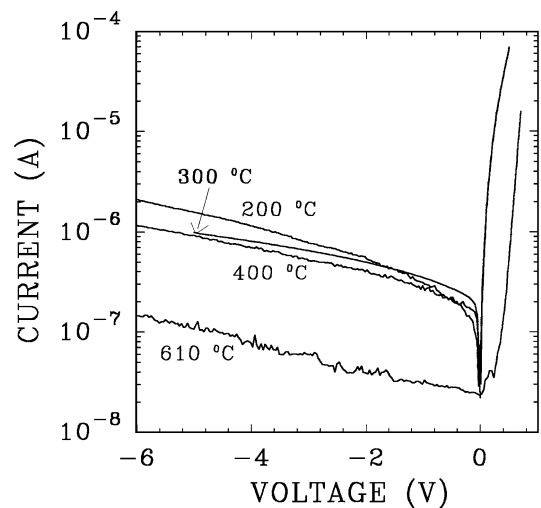


Fig. 1. The *I*-*V* characteristics at 376 K for the samples grown at 200, 300, 400 and 610°C.

from modified emission time τT^2 versus $1000/T$, the activation energies (capture cross sections) were obtained to be 0.66 eV ($1.1 \times 10^{-11} \text{ cm}^2$), 0.66 eV ($5.6 \times 10^{-11} \text{ cm}^2$) and 0.74 eV ($1.5 \times 10^{-10} \text{ cm}^2$) for the samples grown at 200, 300 and 400°C, respectively.

To show that this capacitance dispersion is affected by the large resistivity due to the LT growth, let us refer to a simplified band diagram and its equivalent circuit in Fig. 3, where an acceptor trap is assumed in the LT layer. Analysis of the equivalent circuit yields the capacitance:

$$C(\omega) = \frac{C_1 C_2}{C_1 + C_2} \left[1 + \frac{C_2 / C_1}{1 + \omega^2 R^2 (C_1 + C_2)^2} \right]$$

where R and $C_1 = A\epsilon/d = 120 \text{ pF}$ represent the resistivity and geometric capacitance of the highly-resistive LT layer (0.2 μm) and $C_2 = 40 \text{ pF}$ is the geometric depletion capacitance for the intrinsic layer (0.6 μm). At high frequencies where $1/\omega \ll (C_1 + C_2)R$, only the free carriers on both edges of *n* and *p* regions can be modulated, the high-frequency capacitance reduces to $C_h = C_1 C_2 / (C_1 + C_2) = 30 \text{ pF}$ which is equal to the experimental high-frequency capacitance as shown in Fig. 2 for samples grown at 200, 300 and 400°C.

When the signal frequency is sufficiently low, the electrons

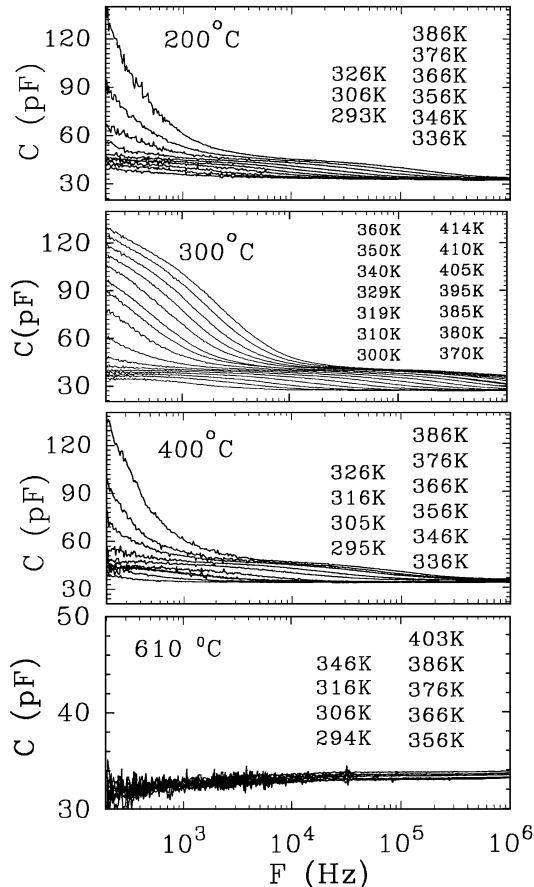


Fig. 2. The C-F spectra at a bias of -2V for the samples grown at 200, 300, 400 and 610°C .

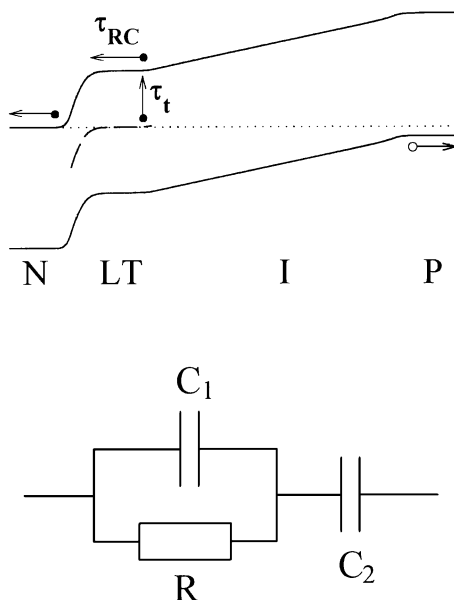


Fig. 3. The simplified band diagram where a trap is assumed in the LT layer and its corresponding equivalent circuit.

are emitted from traps at the edge of the LT layer with an emission time constant τ_t and traverse through the highly-resistive LT layer with a time constant $\tau_{RC} = R(C_1 + C_2)$. Because the large R for the LT layer, let us assume that $R(C_1 + C_2) > \tau_t$, therefore, the capacitance drops at the inflexion frequency $\omega = \tau^{-1} = [R(C_1 + C_2)]^{-1}$. By fitting to

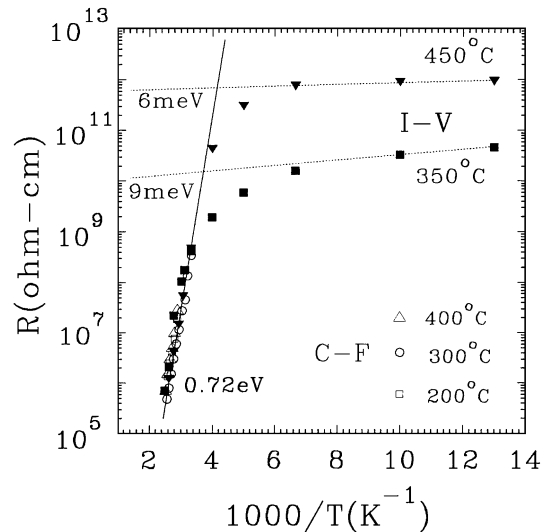


Fig. 4. The resistivities from the C-F spectra (hollow points) and from the $I-V$ analysis of the $n^+\text{-LT-n}^+$ structures (solid points).

the inflexion frequency in Fig. 2, the resistivities R were obtained and are shown as the hollow points in Fig. 4. Similar resistivities were obtained for the samples grown at 200, 300 and 400°C . They are about $10^8 \Omega \cdot \text{cm}$ at 300 K and decrease to about $10^6 \Omega \cdot \text{cm}$ at 400 K. These values were found to be in agreement with the resistivities measured from the $I-V$ analysis of $n^+\text{-LT-n}^+$ structures⁵⁾ with LT layers grown at 350°C (solid squares) and 450°C (solid triangles). This agreement confirms that the high-frequency capacitance dispersion is the result of the $R(C_1 + C_2)$ time constant effects. Any electrons emitted from traps with emission time shorter than $R(C_1 + C_2)$ will show this time constant in the C-F spectra. Because of the large resistivity of the LT layer, this effect is expected to occur in any ac capacitance measurement. Therefore, care must be taken to analyze the data such as the capture cross sections either from capacitance-frequency or deep-level transient spectroscopy measurements.⁸⁾ As for the obtained activation energies (0.66–0.74 eV) for samples grown at 200, 300 and 400°C , they should be the activation energies of the resistivity R of the LT layers, in which traps locate at this energy below the conduction band. The activation energy obtained here is thought to be the mid-gap traps previously observed in LT-grown GaAs, such as the 0.65 eV trap reported by Look *et al.*,⁹⁾ the trap at 0.64 eV by Shiobara *et al.*,¹⁰⁾ and the trap at 0.65 eV by Goo *et al.*¹¹⁾

As previously discussed, the low-, mid- and high-frequency capacitance each measure the thickness of the LT layer, intrinsic layer and the sum of these two layers. We can use the mid-frequency capacitance versus reverse voltage characteristics shown in Fig. 5 to estimate the concentration of the traps. The inset of Fig. 5 shows the low-, mid- and high-frequency capacitance as a function of the reverse voltage for the sample grown at 300°C . When the reverse voltage increases, the mid-frequency capacitance decreases, implying the expansion of the intrinsic layer, which in turn decreases the effective thickness of the LT layer, causing the low-frequency capacitance to increase as shown. Assuming the decrease in the effective thickness of the LT layer is the result of the electron depletion in traps at the edge of the LT layer, neglecting any depletion in the p-type electrode, the concentration of traps occupied

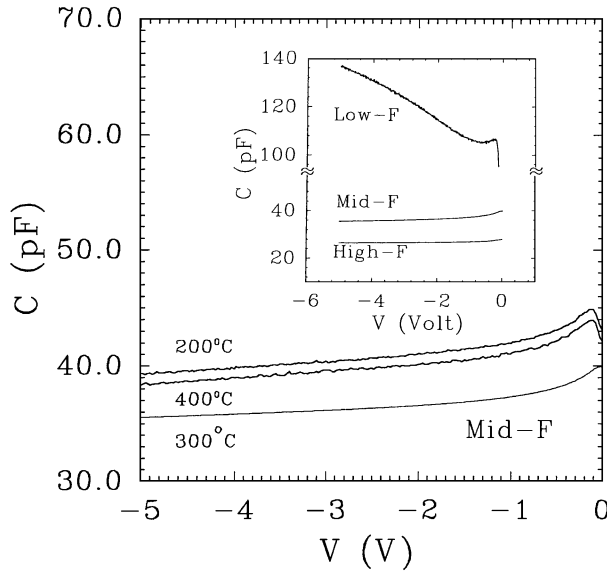


Fig. 5. The mid-frequency capacitance versus reverse voltage characteristics for samples grown at 200, 300 and 400°C. Shown in the inset is the low-, mid- and high-frequency capacitance versus the reverse voltage for the sample grown at 300°C.

by electrons can be roughly estimated from the following expression⁷⁾

$$\frac{1}{C} \frac{\partial C}{\partial V} = - \left(\frac{\epsilon_S}{qd^2} \right) \frac{1}{N_t},$$

where V is the potential difference across the intrinsic layer. Figure 5 reveals that the samples grown at 200, 300 and 400°C have similar $C-V$ slopes, implying that they have similar concentrations of occupied traps which were roughly estimated to be $(3 \pm 1) \times 10^{17} \text{ cm}^{-3}$. This phenomenon of similar concentration of traps is consistent with that of similar resistivities found for these three samples.

We can also estimate the trap concentration from analyzing the resistivity of the $n^+ \text{-LT-} n^+$ structures shown in Fig. 4. According to Mott and Twose¹²⁾ and Shkllovskii,¹³⁾ the nearest neighbor hopping conduction at low temperatures can be given by

$$\rho \approx \rho_0 \exp \left(\frac{1.8}{N_t^{1/3} a} \right) \exp \left(\frac{\alpha \frac{q^2 N_t^{1/3}}{4\pi\epsilon}}{kT} \right)$$

where ρ_0 and α are constants. To obtain the trap concentration, let us fit the asymptote resistivity at high temperatures, that is

$$\rho(T \rightarrow \infty) = \rho_0 \exp \left(\frac{1.8}{N_t^{1/3} a} \right),$$

here ρ_0 was reported to be about $10^{-3} \Omega \cdot \text{cm}$.^{1,13)} As shown in Fig. 4, $\rho(T \rightarrow \infty) \approx 10^{10} \Omega \cdot \text{cm}$ for the 350°C-grown sample and $\rho(T \rightarrow \infty) \approx 10^{12} \Omega \cdot \text{cm}$ for the 450°C-grown sample, the trap concentration N_t was determined to be $3 \times 10^{17} \text{ cm}^{-3}$ ($2 \times 10^{17} \text{ cm}^{-3}$) for the 350°C-grown (450°C-grown) sample. We can also fit the activation energy of the resistivity to obtain the trap concentration using

$$E_a \approx \alpha \frac{q^2 N_t^{1/3}}{4\pi\epsilon},$$

where α depends on the degree of defect compensation. For low compensation, $\alpha = 0.99(1 - 0.3K^{1/4})$, where K represents the compensation level. For high compensation, $\alpha = (1 - 0.3K^{11/3})^{-1}$. Therefore, choosing $\alpha = 1$ and from $E_a \approx 9 \text{ meV}$ ($\approx 6 \text{ meV}$), N_t was determined to be $5.5 \times 10^{17} \text{ cm}^{-3}$ ($1.6 \times 10^{17} \text{ cm}^{-3}$) for the 350°C-grown (450°C-grown) sample. This result indicates that the trap concentrations estimated by both methods are consistent with those estimated from the mid-frequency $C-V$ curve. This consistency provides another evidence for the validity of the assumed band diagram and its equivalent circuit.

The authors would like to thank the National Science Council of the Republic of China for providing financial support for this work under Contract No. NSC-87-2112-M-009-022.

- 1) D. C. Look, D. C. Walters, M. O. Manasreh, J. R. Sizelove and C. E. Stutz: Phys. Rev. B **42** (1990) 3578.
- 2) A. C. Warren, J. M. Woodall, J. L. Freeouf, D. Grischkowsky, D. T. McInturff, M. R. Melloch and N. Otsuka: Appl. Phys. Lett. **57** (1990) 1331.
- 3) X. Liu, A. Prasad, J. Nishio, E. R. Weber, Z. Liliental-Weber and W. Walukiewicz: Appl. Phys. Lett. **67** (1995) 279.
- 4) M. Kaminska, Z. Liliental-Weber, E. R. Weber, T. George, J. B. Kortright, F. W. Smith, B. Y. Tsaur and A. R. Calawa: Appl. Phys. Lett. **54** (1989) 1881.
- 5) T. C. Lin, H. T. Kaibe and T. Okumura: Jpn. J. Appl. Phys. **33** (1994) L1651.
- 6) J. F. Chen, N. C. Chen, S. Y. Chiu, P. Y. Wang, W. I. Lee and A. Chin: J. Appl. Phys. **79** (1996) 8488.
- 7) N. C. Chen, P. Y. Wang and J. F. Chen: J. Appl. Phys. **83** (1998) 1403.
- 8) J. F. Chen, P. Y. Wang and N. C. Chen: Jpn. J. Appl. Phys. **37** (1998) L1238.
- 9) D. C. Look, Z.-Q. Fang, H. Yamamoto, J. R. Sizelove, M. G. Mier and C. E. Stutz: J. Appl. Phys. **76** (1994) 1029.
- 10) S. Shiobara, T. Hashizume and Hasegawa: Jpn. J. Appl. Phys. **35** (1996) 1159.
- 11) C. H. Goo, W. S. Lau, T. C. Chong and L. S. Tan: Appl. Phys. Lett. **69** (1996) 2543.
- 12) N. F. Mott and W. D. Twose: Adv. Phys. **10** (1961) 107.
- 13) B. I. Shkllovskii: Sov. Phys. Semicond. **6** (1973) 1053.